Research Article Vol. 13, No. 8 / 1 Aug 2023 / Optical Materials Express 2405

Optical Materials EXPRESS

Simultaneously improved hole injection and current uniformity in 293 nm AlGaN-based deep ultraviolet light-emitting diodes

MENGRAN LIU,[1,2] WENTAO TIAN,[1,2] AND CHAO LIU[1,2,*]

[1] *School of Microelectronics, Institute of Novel Semiconductors, Shandong Technology Center of Nanodevices and Integration, State Key Laboratory of Crystal Materials, Shandong University, Jinan 250100, China*

[2] *Shenzhen Research Institute, Shandong University, Shenzhen 518057, China*

[*] *chao.liu@sdu.edu.cn*

Abstract: Insufficient hole injection and current nonuniformity caused by the nature of the p-AlGaN hole injection layer (HIL) are two issues impeding the advances in the optical and electrical properties of AlGaN-based deep ultraviolet light-emitting diodes (DUV LEDs). To simultaneously improve the hole injection efficiency and current uniformity, an Al-linearly-decreasing AlGaN PN junction (ALD AlGaN PN junction) is proposed to replace the conventional p-AlGaN HIL with a constant Al component. The barrier height for holes at the interface between the p-type electron blocking layer (p-EBL) and HIL as well as the hole concentration and resistance in the p-AlGaN HIL can be modulated at the same time by the proposed ALD AlGaN PN junction. As a result, the hole injection efficiency is enhanced due to the reduced barrier height at the p-EBL/HIL interface and the polarization-induced three-dimensional hole gas (3DHG) induced in the proposed ALD AlGaN PN junction HIL. In addition, the lateral current uniformity is improved by the properly regulated resistance in the p-AlGaN HIL, which can be ascribed to the additional barrier for holes in the valence band because of the incorporated ALD AlGaN PN junction. The proposed DUV LED with ALD AlGaN PN junction exhibits enhanced EQE by a factor of 39.2% at 100 A/cm^2 and simultaneously improved current uniformity in the active region. This designed ALD AlGaN PN junction structure provides a promising strategy for achieving high-performance DUV LEDs.

1. Introduction

Mercury-based lamps have been the mainstream deep ultraviolet (DUV) light sources for decades, whereas their bulky volume, long warm-up time, low reliability, and hazards to the environment and humans limit their further and long-term applications. In contrast, the tunable direct bandgap enables AlGaN ternary alloy to be suitable for the fabrication of deep ultraviolet light-emitting diodes (DUV LEDs). AlGaN-based DUV LEDs exhibit small form factors, low power loss, long lifetime, and environmental friendliness, which makes them the most promising light sources in the fields of water/air sterilization and purification, phototherapy, UV curing, biomedical testing, UV communication, and excitonic engineering applications [1–6]. However, the commercialization process of AlGaN-based DUV LEDs is restricted by their unsatisfactory external quantum efficiency (EQE). Despite of the recent progress made towards enhanced EQE of DUV LEDs [7–9], there is still room for further improvement of the device performance. Specifically, the light extraction efficiency (LEE) of DUV LEDs is typically below 10% [1,10,11], which requires comprehensive design strategies of the substrates and p-contact layers [12–14]. In the meantime, extensive research has been devoted to the enhancement of the internal quantum efficiency (IQE) from the aspect of structural optimization and energy band engineering [15]. A p-type electron blocking layer (p-EBL) is commonly introduced between the multiple quantum

#495225 https://doi.org/10.1364/OME.495225
Journal © 2023 Received 9 May 2023; revised 26 Jun 2023; accepted 1 Jul 2023; published 27 Jul 2023

Optical Materials EXPRESS

wells (MQWs) active region and the p-AlGaN hole injection layer (HIL) to suppress the electron overflow from the active region. Nevertheless, the polarization-induced positive sheet charges at the interface between the last quantum barrier (LQB) and p-EBL can block the hole transportation from p-EBL into the active region, limiting the hole injection efficiency of AlGaN-based DUV LEDs [16,17]. Aimed at addressing the aforementioned issue of hole blocking effect at the LQB/p-EBL interface, diversified approaches have been proposed to modify the epitaxial structure of LQB and p-EBL [18–21]. In addition, AlN layer [17], AlGaN/AlGaN superlattice [22], and Al-composition-increasing AlGaN layer [23] inserted between the LQB and p-EBL have been reported to modulate the polarization condition at the LQB/p-EBL interface and promote the hole injection efficiency. Except for the hole blocking effect due to the positive sheet charges generated by polarization, the barrier height for holes at the p-EBL/HIL interface, which can be attributed to the valence band discontinuity, is another essential factor that restricts the hole injection from p-type region into the MQWs region [2]. In addition, the large ionization energy of Mg leads to low acceptor ionization rate and consequent poor electrical conductivity in Al-rich p-AlGaN HIL of DUV LEDs [24–26], which is unfavourable for the hole injection and lateral current uniformity [27]. Moreover, the issue of current nonuniformity gives rise to inhomogeneous luminescence and local Joule heating effect, thus bringing about increased junction temperature, local hot-spots at the p-contact edge and degraded device reliability [28]. Various schemes have been proposed to promote the hole injection efficiency and enhance the luminous efficiency of DUV LEDs [7,29–32]. Recently, Che et al. proposed to replace the conventional p-AlGaN HIL with AlGaN PNP junctions to improve the lateral current uniformity [33,34]. However, structural design of HIL from the aspect of the polarization doping schemes accompanying current uniformity of DUV LEDs remains to be explored.

In this study, we incorporate an Al-linearly-decreasing AlGaN PN junction (ALD AlGaN PN junction) HIL structure in AlGaN-based DUV LEDs with an attempt to address the issues of hole injection and current nonuniformity simultaneously. On the one hand, the hole injection is enhanced via polarization-induced three-dimensional hole gas (3DHG) and reduced barrier height for holes at the p-EBL/HIL interface for the proposed DUV LED with ALD AlGaN PN junction. On the other hand, the current uniformity is improved due to the slightly increased resistance of the HIL and the extra potential barrier for holes in the valence band generated by the n-type region of the ALD AlGaN PN junction. Therefore, the proposed DUV LED exhibits enhanced EQE by a factor of 39.2% at 100 A/cm^2 by introducing an ALD AlGaN PN junction to replace the conventional p-AlGaN HIL. This structure provides an alternative approach to achieving DUV LEDs with improved luminous efficiency and current uniformity.

2. Device structure and parameters

As displayed in Fig. 1(a), the reference epitaxial structure (denoted as Device A) used for this study is based on the AlGaN-based DUV LED reported by Zhang et al. [35], which consists of a 4 µm-thick n-$Al_{0.6}Ga_{0.4}N$, followed by multiple quantum wells (MQWs) active region with five pairs of $Al_{0.45}Ga_{0.55}N$ quantum well /$Al_{0.57}Ga_{0.43}N$ quantum barrier (3 nm/10 nm), a 10 nm-thick p-$Al_{0.6}Ga_{0.4}N$ EBL, a 50 nm-thick p-$Al_{0.4}Ga_{0.6}N$ HIL, a 50 nm-thick p-GaN, and a 20 nm-thick p^+-GaN from bottom to top. A 200 nm-thick indium tin oxide (ITO) is utilized as the current spreading layer on the top of the p-type region. In order to probe the effects of different modified schemes for HIL structure on the performance of DUV LEDs, the conventional p-$Al_{0.4}Ga_{0.6}N$ HIL of Device A is replaced with the 50 nm-thick p-$Al_{0.5\sim0.3}Ga_{0.5\sim0.7}N$, p-$Al_{0.4}Ga_{0.6}N$/n-$Al_{0.4}Ga_{0.6}N$ (25 nm/25 nm) PN junction and Al-linearly-decreasing p-$Al_{0.5\sim0.4}Ga_{0.5\sim0.6}N$/n-$Al_{0.4\sim0.3}Ga_{0.6\sim0.7}N$ (25 nm/25 nm) PN junction for the proposed Device B, C and D respectively. The mesa sizes of all the studied DUV LEDs are set as 350 µm × 350 µm. The schematic energy band diagram of Device D is presented in Fig. 1(b). It can be observed that 3DHG together with an extra mini barrier for holes are introduced in the valence band of the HIL by the ALD AlGaN PN

Optical Materials EXPRESS

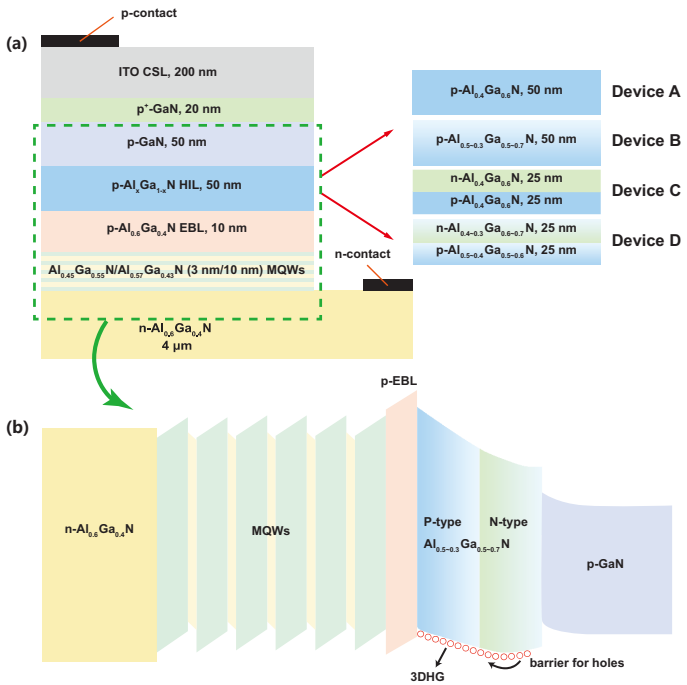

Fig. 1. (a) Sketched structure of the investigated AlGaN-based DUV LEDs and (b) estimated energy band diagram of the distinct region marked by the green box for Device D, in which the doping concentration of n-$Al_{0.6}Ga_{0.4}N$ is 8×10^{18} cm^{-3}, and the p-type layers possess effective hole concentrations of $\sim1\times10^{17}$ cm^{-3}. The conventional p-$Al_{0.4}Ga_{0.6}N$ HIL of Device A is replaced with the p-$Al_{0.5\sim0.3}Ga_{0.5\sim0.7}N$, $Al_{0.4}Ga_{0.6}N$ PN junction and Al-linearly-decreasing $Al_{0.5\sim0.3}Ga_{0.5\sim0.7}N$ PN junction for Device B, C, and D, respectively.

junction, whose impact on the performance of the AlGaN-based DUV LEDs will be analyzed in the following section in more detail.

The numerical simulation procedure was carried out by means of the Advanced Physical Models of Semiconductor Devices (APSYS) software, in which the Poisson's equation, Schrödinger equation, current continuity equation, and drift-diffusion equation are self-consistently solved to calculate related optical and electrical properties of the investigated DUV LEDs [36,37]. During the simulation process, the band offset ratio was set as 50:50 for AlGaN/AlGaN heterojunctions to characterize and compare the energy band diagrams of the investigated DUV LEDs [38]. Besides, the Auger recombination coefficient, Shockley-Read-Hall (SRH) recombination lifetime, and light extraction efficiency used in the numerical simulation were set to be 1.7×10^{-30} cm^6/s [39,40], 14 ns [39], and 6% [1,10,35,41,42] respectively, which is determined by fitting the calculated EQE and optical power to the on-wafer measured results of Device A [35], as shown in Fig. 2(a). The spontaneous and piezoelectric polarization in AlGaN layers is calculated according to the approach reported by Fiorentini et al. in this simulation study [43].

3. Results and discussion

As shown in Fig. 2(a), the calculated EQE and optical power of Device A agree well with the measured results, indicating the effectiveness of the parameters utilized in the simulation. Figure 2(b) and (c) present the calculated EQE and optical power of all the studied devices separately. Compared with Device A, Device B with p-$Al_{0.5\sim0.3}Ga_{0.5\sim0.7}N$ HIL exhibits obviously enhanced EQE and optical power. In contrast, minor enhancement in EQE and optical

Optical Materials EXPRESS

power is observed for Device C with $Al_{0.4}Ga_{0.6}N$ PN junction HIL. After incorporating the $Al_{0.5\sim0.3}Ga_{0.5\sim0.7}N$ PN junction HIL in Device D, further enhanced EQE and optical power are obtained in comparison with Device B, exhibiting the best overall performance among all the proposed devices. Figure 2(d) presents the calculated emission curves of Device A, B, C, and D. It can be observed that the four DUV LEDs all peak at the same wavelength of 293 nm.

Figure 3(a) displays the horizontal hole concentration in the third quantum well of the reference DUV LED and the three proposed DUV LEDs which are denoted as Series I with a p-contact width of 100 µm. The inset shows the integrated horizontal hole concentration of the LEDs for comparison. It can be observed that Device B exhibits significantly enhanced hole concentration compared with Device A, while the hole distribution is less uniform. As for Device C, although the uniformity of the hole concentration is improved, less enhancement in the hole concentration is obtained. In contrast, the hole concentration in the active region is boosted with simultaneously improved current uniformity for Device D, via introducing the proposed ALD AlGaN PN junction structure.

To verify the effectiveness of the ALD AlGaN PN junction HIL in improving the current uniformity, we simulated three additional series of DUV LEDs with increased p-contact widths of 150 µm, 200 µm, and 250 µm (Series II, Series III, and Series IV), respectively. The horizontal hole concentration distribution of the three series of DUV LEDs above is presented in Fig. 3(b), (c), and (d), respectively. Since Device D and Device B both feature significantly enhanced hole concentration in the active region, we further explored the impact of the p-contact width on the current uniformity based on the two types of devices. It can be observed that with increased p-contact width, Device D2, D3, and D4 still exhibit improved current uniformity compared with

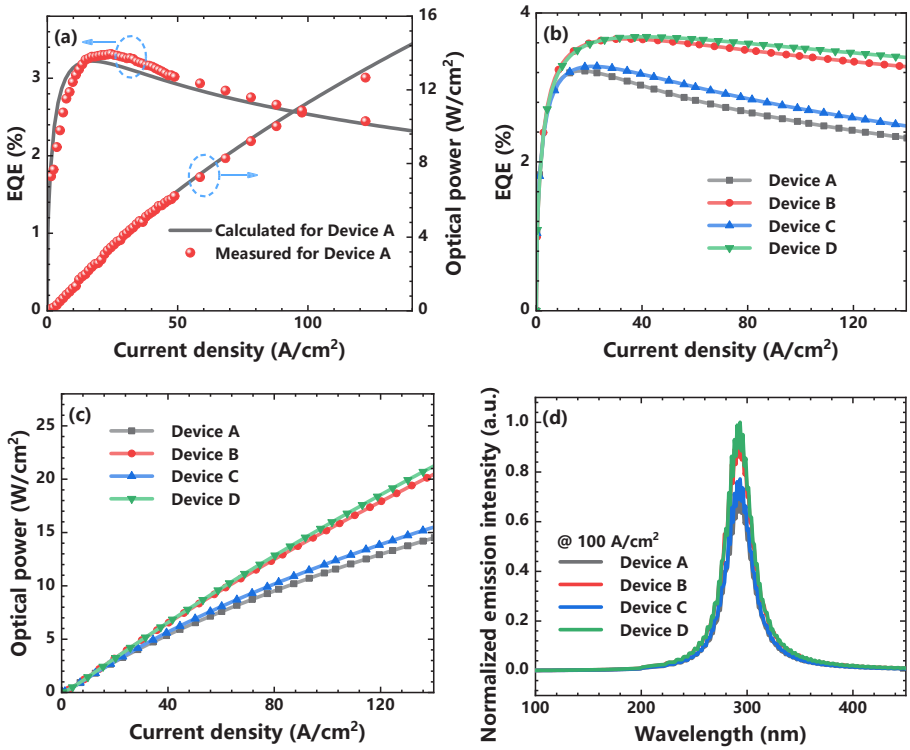

Fig. 2. (a) Calculated and on-wafer measured EQE and optical power as a function of the injection current density of Device A. Calculated (b) EQE, (c) optical power, and (d) normalized emission curves at 100 A/cm^2 for all the studied devices.

Optical Materials EXPRESS

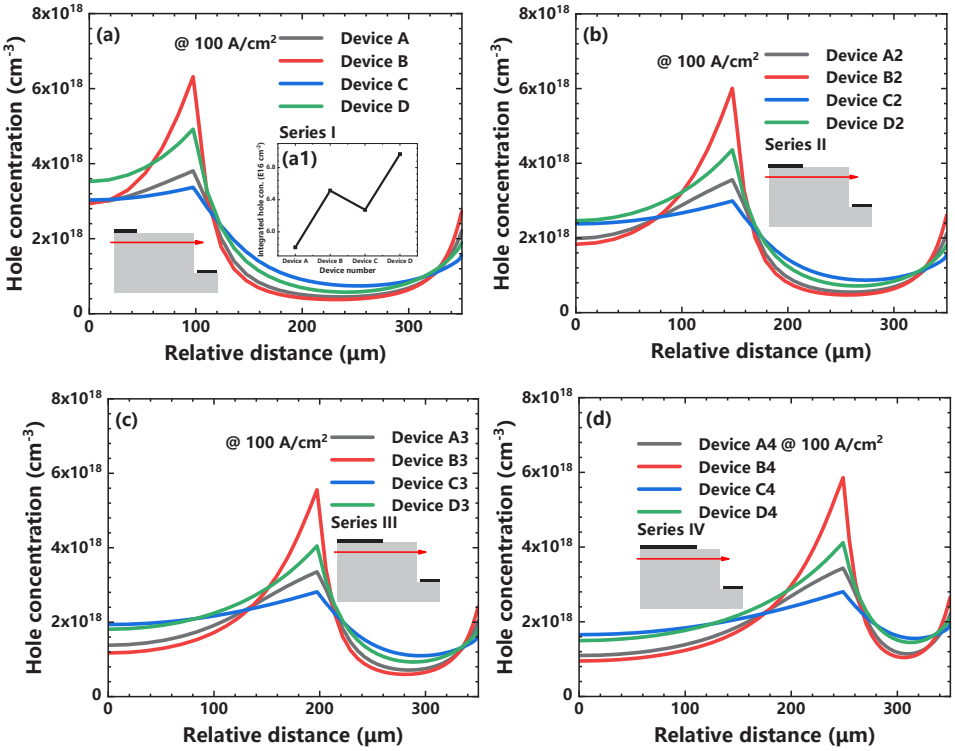

Fig. 3. Horizontal hole concentration in the third quantum well along the horizontal cutline of (a) Series I, (b) Series II, (c) Series III, and (d) Series IV of DUV LEDs at the injection current density of 100 A/cm^2. Note that the p-contact widths for Series I, II, III, and IV are 100 μm, 150 μm, 200 μm, and 250 μm, respectively. Figure 3(a1) shows the integrated horizontal hole concentration (con. for short) of the LEDs for comparison.

Device B2, B3, and B4, confirming the advantage of the proposed ALD AlGaN PN junction HIL structure in mitigating the current spikes at the p-contact edge and promoting the luminescence uniformity as well as the device reliability.

In order to elaborate the underlying mechanism behind the different effects of the proposed HIL structures on the optical and electrical characteristics of DUV LEDs, we presented the schematic illustration of polarization-induced 3DHG in $Al_{0.5\sim0.3}Ga_{0.5\sim0.7}N$ and simplified equivalent circuits, as well as I-V curves and hole concentration in the HILs of all the studied devices. It has been demonstrated that 3DHG can be generated by linearly decreasing the Al composition along the direction of [0001] [44]. As illustrated in Fig. 4(a), the total polarizations in the unit cells of $Al_{0.5\sim0.3}Ga_{0.5\sim0.7}N$ are denoted as charge dipoles which exhibit a linear variation across the graded layer as the Al composition decreases along the [0001] direction. Besides, due to the higher polarization in AlGaN than that in GaN, net negative unbalanced polarization-induced charges are generated, resulting in mobile 3DHG that is determined by $\rho_\pi = \nabla \cdot \boldsymbol{P}$, in which $\nabla\cdot$ and $\boldsymbol{P}$ denote divergence operator and total polarization in $Al_xGa_{1-x}N$ severally. Figure 4(b) presents the hole concentration in the HILs of all the studied devices at the injection current density of 100 A/cm^2. It can be observed that the p-$Al_{0.5\sim0.3}Ga_{0.5\sim0.7}N$ HIL of Device B possesses higher average hole concentration compared to the p-$Al_{0.4}Ga_{0.6}N$ HIL of Device A due to the existence of the polarization-induced 3DHG. On the contrary, the average hole concentration in the $Al_{0.4}Ga_{0.6}N$ PN junction HIL of Device C is lower than that of Device A, which can be ascribed to the hole depletion effect of the n-type part of $Al_{0.4}Ga_{0.6}N$ PN junction. In contrast

Optical Materials EXPRESS

with Device C, in spite of the hole depletion induced by the n-type part of $Al_{0.5\sim0.3}Ga_{0.5\sim0.7}N$ PN junction, the hole concentration in the HIL of Device D is enhanced, indicating the availability of the 3DHG via the proposed Al-decreasing scheme.

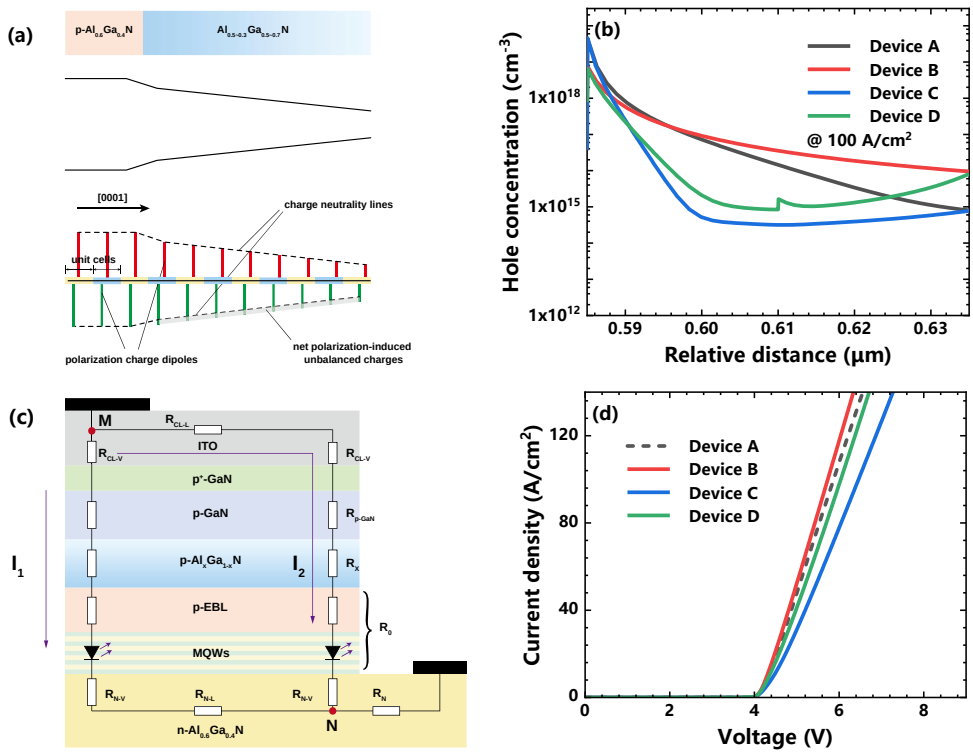

Fig. 4. (a) Schematic illustration of polarization-induced 3DHG in the graded $Al_{0.5\sim0.3}Ga_{0.5\sim0.7}N$ layer. (b) Hole concentration in the HIL structure at the injection current density of 100 A/cm^2, (c) simplified equivalent circuit, and (d) I-V characteristics of all investigated DUV LEDs.

To figure out the reasons for the improved current uniformity for Device C and Device D, we further simplified the equivalent circuits for all the studied devices as shown in Fig. 4(c), in which the total current is divided into the vertical part (I_1) and the lateral part (I_2), both flowing from point M to point N. The voltage drop between M and N can be expressed as [28,34]:

$$U_{MN} = I_1(R_{CL-V} + R_{p-GaN} + R_x + R_0 + R_{N-V} + R_{N-L}) \tag{1}$$

$$U_{MN} = I_2(R_{CL-L} + R_{CL-V} + R_{p-GaN} + R_x + R_0 + R_{N-V}) \tag{2}$$

where R_{CL-L}, R_{CL-V}, R_{p-GaN}, R_x, R_{N-L}, and R_{N-V} represent the horizontal resistance of the current spreading layer (CSL), vertical resistance of CSL, resistance of p-GaN layer, resistance of HIL, horizontal resistance of n-$Al_{0.6}Ga_{0.4}N$, and vertical resistance of n-$Al_{0.6}Ga_{0.4}N$, respectively; R_0 is the sum of the resistances of p-EBL and active region. Note that the resistance of the p^+-GaN contact layer can be neglected due to its high doping concentration and thin thickness. By solving Eqs. (1) and (2), the ratio of I_1 to I_2 can be expressed as:

$$\frac{I_1}{I_2} = 1 + \frac{R_{CL-L} - R_{N-L}}{R_{CL-V} + R_{p-GaN} + R_x + R_0 + R_{N-V} + R_{N-L}} \tag{3}$$

Optical Materials EXPRESS

Therefore, the ratio of I_1/I_2 can be tuned by modulating the resistance of the HIL (R_x). To probe the effects of the proposed structures on the I-V characteristics, we plotted the I-V curves of all studied DUV LEDs, as shown in Fig. 4(d). It can be observed that the dynamic resistance of Device B is reduced via utilizing the p-$Al_{0.5\sim0.3}Ga_{0.5\sim0.7}N$ HIL, while increased dynamic resistances are obtained for Device C and Device D owing to the introduction of n-type AlGaN layer in HIL. Besides, R_{CL-L} is larger than R_{N-V} due to the fact that the CSL is much thinner than n-$Al_{0.6}Ga_{0.4}N$ electron injection layer. Hence, I_1/I_2 is increased for Device B yet decreased for Device C and Device D, indicating that a larger amount of current is spread along the horizontal direction in Device C and D.

We presented the energy band diagrams and corresponding electric field of the four DUV LEDs in Fig. 5(a), (b), (c), and (d) to further illustrate the underlying mechanism behind the different effects of the proposed HIL structures on the hole injection and current uniformity of DUV LEDs. Apart from the 3DHG induced by the linear change in polarization, the increased initial Al composition of HIL at the p-EBL/HIL interface for Device B contributes to obviously reduced band discontinuity and barrier height of 116.3 meV for holes compared with Device A, further facilitating holes to be injected from HIL into the active region. As shown in Fig. 5(c), in spite of the hole depletion induced by the ionized donors of n-$Al_{0.4}Ga_{0.6}N$ layer in HIL, Device C exhibits larger negative electric field in HIL, which is beneficial to hole transportation, resulting in enhanced hole concentration and luminous efficiency in the active region compared with Device A [22,45]. In contrast, Device D not only exhibits reduced barrier height for holes at the p-EBL/HIL interface but also possesses polarization-induced 3DHG and larger negative electric field in HIL compared with Device A, thus obtaining the highest hole concentration in the active

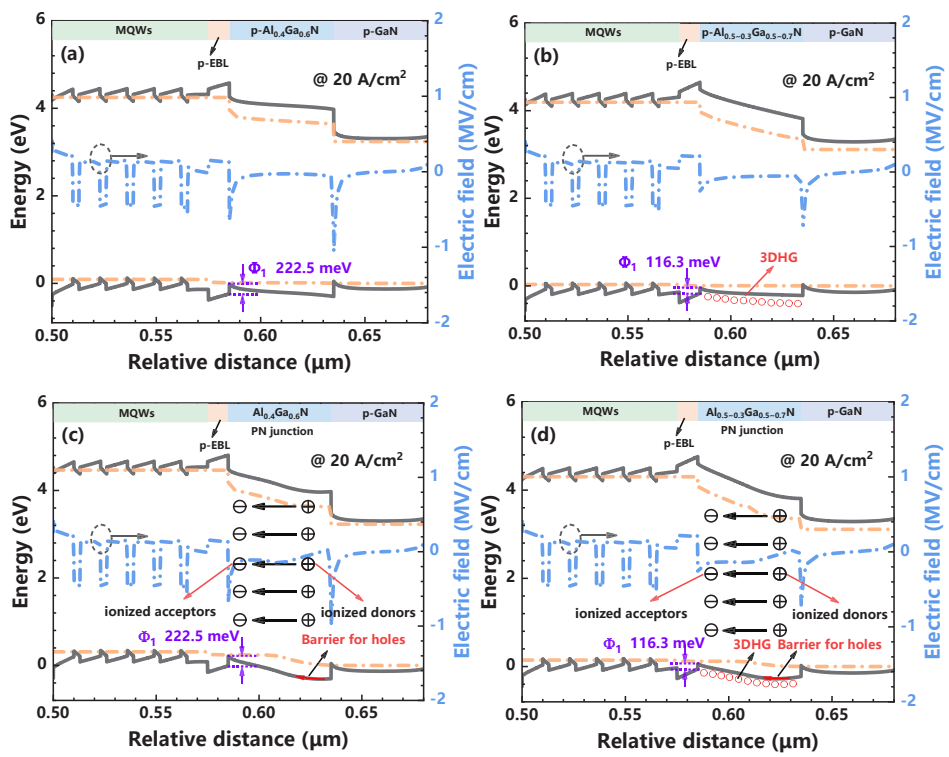

Fig. 5. Calculated energy band diagram and electric field of (a) Device A, (b) Device B, (c) Device C, and (d) Device D at 20 A/cm^2.

Optical Materials EXPRESS

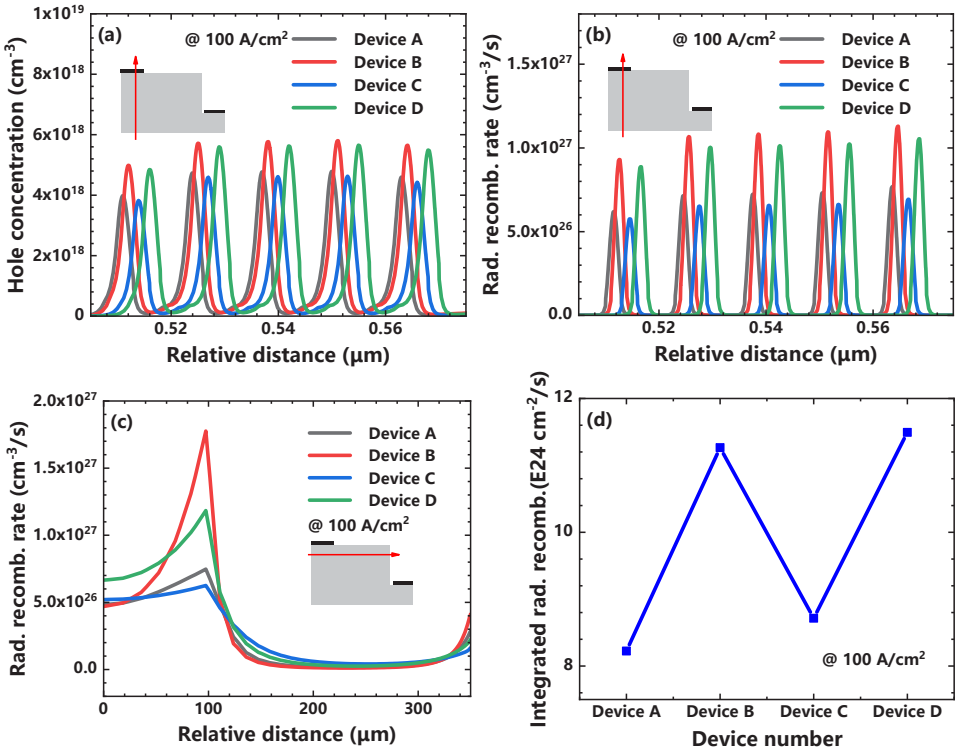

Fig. 6. (a) Hole concentration and (b) radiative (rad. for short) recombination rates in the active region along the vertical cutline of all the studied devices at 100 A/cm^2. (c) Horizontal radiative recombination rates, and (d) integrated horizontal radiative recombination rates in the third quantum well along the horizontal cutline of Device A, B, C, and D at 100 A/cm^2. To make a clear comparison, the horizontal positions of the hole concentration curves and radiative recombination rates curves in Fig. 6(a) and (b) are shifted rightwards by 1 nm, 3 nm, and 5 nm for Device B, C, and D, respectively.

region. Furthermore, an extra potential barrier in the valence band of HIL is generated in Device C and Device D due to the introduction of n-type AlGaN layer, which pushes more holes to transport along the horizontal direction instead of vertical direction [33] and partly accounts for the increased resistance of HIL. Therefore, the ratio of the lateral current is enhanced, mitigating the current nonuniformity for Device C and Device D.

To demonstrate the influence of the proposed design strategies of HIL structures on the optical property of AlGaN-based DUV LEDs, we extracted the hole concentration and radiative recombination rates in the active region along the vertical cutline of all the studied devices, as shown in Fig. 6(a) and (b). The quantum wells exhibit good hole confinement thanks to the sufficient Al-alloy difference of 12% between QB and QW, which is in line with the results from Ref. [46]. Both Device B and Device D exhibit significantly enhanced hole concentration and radiative recombination rates compared with the reference DUV LED. On the contrary, lower hole concentration and radiative recombination rates can be observed in Device C with an $Al_{0.4}Ga_{0.6}N$ PN junction HIL. Figure 6(c) shows the horizontal radiative recombination rates along the horizontal cutline. For a more explicit comparison, we calculated the integrated horizontal radiative recombination rates, as presented in Fig. 6(d). Due to the polarization-induced 3DHG and decreased barrier height for holes at the p-EBL/HIL interface, enhanced hole concentration and consequent boosted radiative recombination rates are achieved for Device B, while the

Optical Materials EXPRESS

recombination rates are less uniform due to the severe current nonuniformity. Although simply incorporating n-type layer in HIL for Device C can improve the lateral uniformity of the hole concentration and radiative recombination rates, the integrated hole concentration and radiative recombination rates in the active region are inferior to those of Device B, as shown in Fig. 3(a1) and Fig. 6(d). With an $Al_{0.5\sim0.3}Ga_{0.5\sim0.7}N$ PN junction implemented as HIL for Device D, the highest overall horizontal hole concentration and radiative recombination rates, together with improved current uniformity in the active region among all the DUV LEDs are achieved thanks to the polarization-induced 3DHG, obviously decreased barrier height for holes at the p-EBL/HIL interface, and simultaneously regulated resistance of HIL.

4. Conclusion

In conclusion, we propose and compare three structural design strategies for the hole injection layer of AlGaN-based DUV LEDs. The proposed DUV LED with an Al-linearly-decreasing $Al_{0.5\sim0.3}Ga_{0.5\sim0.7}N$ PN junction HIL structure exhibits enhanced hole injection efficiency and simultaneously improved current uniformity, which results in enhanced EQE and optical power as well as mitigated hot-spot at the p-contact edge. However, the graded PN junction HIL structure leads to a minor degradation in the I-V characteristics due to the extra barrier introduced in the valence band of HIL. We believe that the proposed Al-linearly-decreasing AlGaN PN junction structure can expand the potential of AlGaN-based DUV LEDs in various applications, including sterilization and purification, medical treatment, biomedical testing, and UV communication.

Funding. Shenzhen Science and Technology Program (JCYJ20210324141212030, GJHZ20210705142537002); Guangdong Basic and Applied Basic Research Foundation (2023A1515011142, 2020A1515111018); Shandong Provincial Natural Science Foundation (ZR2020QF079); Qilu Young Scholar program (11500089963075).

Acknowledgments. The authors thank staff from Simucal Inc. for their fruitful discussion.

Disclosures. The authors declare no conflicts of interest.

Data availability. Data underlying the results presented in this paper are not publicly available at this time but may be obtained from the authors upon reasonable request.

References

1. H. Hirayama, N. Maeda, S. Fujikawa, S. Toyoda, and N. Kamata, "Recent progress and future prospects of AlGaN-based high-efficiency deep-ultraviolet light-emitting diodes," Jpn. J. Appl. Phys. **53**(10), 100209 (2014).
2. M. Kneissl, T. Y. Seong, J. Han, and H. Amano, "The emergence and prospects of deep-ultraviolet light-emitting diode technologies," Nat. Photonics **13**(4), 233–244 (2019).
3. Y. Nagasawa and A. Hirano, "Review of encapsulation materials for AlGaN-based deep-ultraviolet light-emitting diodes," Photonics Res. **7**(8), B55–B65 (2019).
4. C. S. Chu, K. K. Tian, Y. H. Zhang, W. G. Bi, and Z. H. Zhang, "Progress in external quantum efficiency for III-nitride based deep ultraviolet light-emitting diodes," Phys. Status Solidi A **216**(4), 1800815 (2019).
5. X. Y. He, E. Y. Xie, M. S. Islim, A. A. Purwita, J. J. D. McKendry, E. D. Gu, H. Haas, and M. D. Dawson, "1 Gbps free-space deep-ultraviolet communications based on III-nitride micro-LEDs emitting at 262 nm," Photonics Res. **7**(7), B41–B47 (2019).
6. H. Murotani, R. Tanabe, K. Hisanaga, A. Hamada, K. Beppu, N. Maeda, M. A. Khan, M. Jo, H. Hirayama, and Y. Yamada, "High internal quantum efficiency and optically pumped stimulated emission in AlGaN-based UV-C multiple quantum wells," Appl. Phys. Lett. **117**(16), 162106 (2020).
7. M. A. Khan, N. Maeda, J. Yun, M. Jo, Y. Yamada, and H. Hirayama, "Achieving 9.6% efficiency in 304 nm p-AlGaN UVB LED via increasing the holes injection and light reflectance," Sci. Rep. **12**(1), 2591 (2022).
8. M. Shatalov, W. Sun, A. Lunev, X. Hu, A. Dobrinsky, Y. Bilenko, J. Yang, M. Shur, R. Gaska, C. Moe, G. Garrett, and M. Wraback, "AlGaN Deep-Ultraviolet Light-Emitting Diodes with External Quantum Efficiency above 10%," Appl. Phys. Express **5**(8), 082101 (2012).
9. T. Takano, T. Mino, J. Sakai, N. Noguchi, K. Tsubaki, and H. Hirayama, "Deep-ultraviolet light-emitting diodes with external quantum efficiency higher than 20% at 275 nm achieved by improving light-extraction efficiency," Appl. Phys. Express **10**(3), 031002 (2017).
10. H.-Y. Ryu, I.-G. Choi, H.-S. Choi, and J.-I. Shim, "Investigation of light extraction efficiency in AlGaN deep-ultraviolet light-emitting diodes," Appl. Phys. Express **6**(6), 062101 (2013).

Optical Materials EXPRESS

11. G. D. Hao, N. Tamari, T. Obata, T. Kinoshita, and S. I. Inoue, "Electrical determination of current injection and internal quantum efficiencies in AlGaN-based deep-ultraviolet light-emitting diodes," Opt. Express **25**(16), A639–A648 (2017).
12. R. Liang, J. Dai, L. Xu, J. He, S. Wang, Y. Peng, H. Wang, L. Ye, and C. Chen, "High light extraction efficiency of deep ultraviolet LEDs enhanced using nanolens arrays," IEEE Trans. Electron Devices **65**(6), 2498–2503 (2018).
13. D. Lee, J. W. Lee, J. Jang, I.-S. Shin, L. Jin, J. H. Park, J. Kim, J. Lee, H.-S. Noh, Y.-I. Kim, Y. Park, G.-D. Lee, Y. Park, J. K. Kim, and E. Yoon, "Improved performance of AlGaN-based deep ultraviolet light-emitting diodes with nano-patterned AlN/sapphire substrates," Appl. Phys. Lett. **110**(19), 191103 (2017).
14. N. Maeda and H. Hirayama, "Realization of high-efficiency deep-UV LEDs using transparent p-AlGaN contact layer," Phys. Status Solidi C **10**(11), 1521–1524 (2013).
15. H. Murotani, H. Miyoshi, R. Takeda, H. Nakao, M. Ajmal Khan, N. Maeda, M. Jo, H. Hirayama, and Y. Yamada, "Correlation between excitons recombination dynamics and internal quantum efficiency of AlGaN-based UV-A multiple quantum wells," J. Appl. Phys. **128**(10), 105704 (2020).
16. Z. H. Zhang, C. S. Chu, C. H. Chiu, T. C. Lu, L. P. Li, Y. H. Zhang, K. K. Tian, M. Q. Fang, Q. Sun, H. C. Kuo, and W. G. Bi, "UVA light-emitting diode grown on Si substrate with enhanced electron and hole injections," Opt. Lett. **42**(21), 4533–4536 (2017).
17. C. S. Chu, K. K. Tian, J. M. Che, H. Shao, J. Q. Kou, Y. H. Zhang, Y. Li, M. Y. Wang, Y. H. Zhu, and Z. H. Zhang, "On the origin of enhanced hole injection for AlGaN-based deep ultraviolet light-emitting diodes with AlN insertion layer in p-electron blocking layer," Opt. Express **27**(12), A620–A628 (2019).
18. Z. H. Zhang, S. W. H. Chen, Y. H. Zhang, L. P. Li, S. W. Wang, K. K. Tian, C. S. Chu, M. Q. Fang, H. C. Kuo, and W. G. Bi, "Hole transport manipulation to improve the hole injection for deep ultraviolet light-emitting diodes," ACS Photonics **4**(7), 1846–1850 (2017).
19. B. So, J. Kim, T. Kwak, T. Kim, J. Lee, U. Choi, and O. Nam, "Improved carrier injection of AlGaN-based deep ultraviolet light emitting diodes with graded superlattice electron blocking layers," RSC Adv. **8**(62), 35528–35533 (2018).
20. P. Du, L. Shi, S. Liu, and S. J. Zhou, "High-performance AlGaN-based deep ultraviolet light-emitting diodes with different types of InAlGaN/AlGaN electron blocking layer," Jpn. J. Appl. Phys. **60**(9), 092001 (2021).
21. Z. L. Liu, H. B. Yu, Z. J. Ren, J. N. Dai, C. Q. Chen, and H. D. Sun, "Polarization-engineered AlGaN last quantum barrier for efficient deep-ultraviolet light-emitting diodes," Semicond. Sci. Technol. **35**(7), 075021 (2020).
22. M. R. Liu, Y. C. Ji, H. Zhou, C. S. Xia, Z. H. Zhang, and C. Liu, "Sheet charge engineering towards an efficient hole injection in 290 nm deep ultraviolet light-emitting diodes," IEEE Photonics J. **13**(4), 1–8 (2021).
23. M. R. Liu and C. Liu, "Enhanced carrier injection in AlGaN-based deep ultraviolet light-emitting diodes by polarization engineering at the LQB/p-EBL interface," IEEE Photonics J. **14**(3), 1–5 (2022).
24. A. Khan, K. Balakrishnan, and T. Katona, "Ultraviolet light-emitting diodes based on group three nitrides," Nat. Photonics **2**(2), 77–84 (2008).
25. Y. H. Liang and E. Towe, "Progress in efficient doping of high aluminum-containing group III-nitrides," Appl. Phys. Rev. **5**(1), 011107 (2018).
26. K. H. Kim, T. H. Lee, K. R. Son, and T. G. Kim, "Performance improvements in AlGaN-based ultraviolet light-emitting diodes due to electrical doping effects," Mater. Des. **153**, 94–103 (2018).
27. C. S. Chu, Q. Chen, K. K. Tian, J. M. Che, H. Shao, J. Q. Kou, Y. H. Zhang, C. Q. Chen, Z. H. Zhang, and J. N. Dai, "Modulating the layer resistivity by band-engineering to improve the current spreading for DUV LEDs," IEEE Photonics Technol. Lett. **31**(15), 1201–1204 (2019).
28. J. M. Che, H. Shao, J. Q. Kou, K. K. Tian, C. S. Chu, X. Hou, Y. H. Zhang, Q. Sun, and Z. H. Zhang, "Improving the current spreading by locally modulating the doping type in the n-AlGaN layer for AlGaN-based deep ultraviolet light-emitting diodes," Nanoscale Res. Lett. **14**(1), 268 (2019).
29. M. A. Khan, Y. Itokazu, N. Maeda, M. Jo, Y. Yamada, and H. Hirayama, "External quantum efficiency of 6.5% at 300 nm emission and 4.7% at 310 nm emission on bare wafer of AlGaN-based UVB LEDs," ACS Appl. Electron. Mater. **2**(7), 1892–1907 (2020).
30. M. A. Khan, J. P. Bermundo, Y. Ishikawa, H. Ikenoue, S. Fujikawa, E. Matsuura, Y. Kashima, N. Maeda, M. Jo, and H. Hirayama, "Impact of Mg level on lattice relaxation in a p-AlGaN hole source layer and attempting excimer laser annealing on p-AlGaN HSL of UVB emitters," Nanotechnology **32**(5), 055702 (2021).
31. M. Ajmal Khan, N. Maeda, H. Rangaraju, M. Jo, K. Iimura, and H. Hirayama, "Efficiency droop in AlGaN crystal-based UVB LEDs in the context of electron blocking mechanism," J. Cryst. Growth **604**, 127032 (2023).
32. M. Usman, S. Malik, M. A. Khan, and H. Hirayama, "Suppressing the efficiency droop in AlGaN-based UVB LEDs," Nanotechnology **32**(21), 215703 (2021).
33. J. M. Che, H. Shao, L. Chang, J. Q. Kou, K. K. Tian, C. S. Chu, Y. H. Zhang, W. G. Bi, and Z. H. Zhang, "Doping-induced energy barriers to improve the current spreading effect for AlGaN-based ultraviolet-B light-emitting diodes," IEEE Electron Device Lett. **41**(7), 1001–1004 (2020).
34. J. M. Che, C. S. Chu, K. K. Tian, J. Q. Kou, H. Shao, Y. H. Zhang, W. G. Bi, and Z. H. Zhang, "On the p-AlGaN/n-AlGaN/p-AlGaN current spreading layer for AlGaN-based deep ultraviolet light-emitting diodes," Nanoscale Res. Lett. **13**(1), 355 (2018).

Optical Materials EXPRESS

35. D. Y. Zhang, C. S. Chu, K. K. Tian, J. Q. Kou, W. G. Bi, Y. H. Zhang, and Z. H. Zhang, "Improving hole injection from p-EBL down to the end of active region by simply playing with polarization effect for AlGaN based DUV light-emitting diodes," AIP Adv. **10**(6), 065032 (2020).
36. [Online]. Available: http://www.crosslight.com/. Accessed: June 2019.
37. Q. Chen, J. Zhang, Y. Geo, J. W. Chen, H. L. Long, J. N. Dai, Z. H. Zhang, and C. Q. Chen, "Improved the AlGaN-Based ultraviolet LEDs performance with super-lattice structure last barrier," IEEE Photonics J. **10**(4), 1–7 (2018).
38. J. Piprek, "Ultra-violet light-emitting diodes with quasi acceptor-free AlGaN polarization doping," Opt. Quantum Electron. **44**(3-5), 67–73 (2012).
39. M. K. A. J. Rass, "A brief review of III-Nitride UV emitter technologies and their applications," *III-Nitride Ultraviolet Emitters: Technology and Applications* (Springer, 2016), pp. 1–25.
40. E. Kioupakis, P. Rinke, K. T. Delaney, and C. G. Van de Walle, "Indirect Auger recombination as a cause of efficiency droop in nitride light-emitting diodes," Appl. Phys. Lett. **98**(16), 161107 (2011).
41. S. H. Lin, M. C. Tseng, K. W. Peng, S. Q. Lai, M. C. Shen, R. H. Horng, S. Y. Lien, D. S. Wuu, H. C. Kuo, T. Z. Wu, and Z. Chen, "Enhanced external quantum efficiencies of AlGaN-based deep-UV LEDs using reflective passivation layer," Opt. Express **29**(23), 37835–37844 (2021).
42. N. Maeda, J. Yun, M. Jo, and H. Hirayama, "Enhancing the light-extraction efficiency of AlGaN deep-ultraviolet light-emitting diodes using highly reflective Ni/Mg and Rh as p-type electrodes," Jpn. J. Appl. Phys. **57**(4S), 04FH08 (2018).
43. V. Fiorentini, F. Bernardini, and O. Ambacher, "Evidence for nonlinear macroscopic polarization in III-V nitride alloy heterostructures," Appl. Phys. Lett. **80**(7), 1204–1206 (2002).
44. J. Simon, V. Protasenko, C. X. Lian, H. L. Xing, and D. Jena, "Polarization-induced hole doping in wide-band-gap uniaxial semiconductor heterostructures," Science **327**(5961), 60–64 (2010).
45. Z. H. Zhang, L. P. Li, Y. H. Zhang, F. J. Xu, Q. Shi, B. Shen, and W. G. Bi, "On the electric-field reservoir for III-nitride based deep ultraviolet light-emitting diodes," Opt. Express **25**(14), 16550–16559 (2017).
46. M. A. Khan, R. Takeda, Y. Yamada, N. Maeda, M. Jo, and H. Hirayama, "Beyond 53% internal quantum efficiency in a AlGaN quantum well at 326 nm UVA emission and single-peak operation of UVA LED," Opt. Lett. **45**(2), 495–498 (2020).